In-Situ Nanocomposite Synthesis: Arylcarbonylation and Grafting of Primary Diamond Nanoparticles with a Poly(ether−ketone) in Polyphosphoric Acid

David H. Wang,[†] Loon-Seng Tan,*[,‡] Houjin Huang,[§] Liming Dai,[§] and Eiji Ōsawa[‖]

University of Dayton Research Institute, 300 College Park, Dayton, Ohio 45469-0060; Nanostructured & Biological Materials Branch, Materials and Manufacturing Directorate Air Force Research Laboratory, AFRL/RXBN, Wright-Patterson AFB, Ohio 45433-7750; Department of Chemical and Materials Engineering, University of Dayton, 300 College Park, Dayton, Ohio 45469; and NanoCarbon Research Institute, Ltd., Asama Research Extension Centre, Faculty of Textile Science & Technology, Shinshu University, 3-15-1 Tokita, Ueda, Nagano 386-8567, Japan

ABSTRACT: In a model reaction to demonstrate the presence and reactivity of sp^2 C−H, the primary particles (~5 nm) of detonation nanodiamond (DND) were arylcarbonylated with 2,4,6-trimethylphenoxybenzoic acid in polyphosphoric acid (PPA) via a Friedel−Crafts reaction. The possibility of grafting primary DND particle was supported by the results from FTIR, scanning electron microscopy (SEM), and elemental analysis. From the latter result, we estimated the degree of functionalization to be ~2.3 atom %. The arylcarbonylated DND achieved better and stable dispersion than pristine DND in common organic solvents. PPA-treated DND from the control experiment retained most of the pristine DND's properties, except that its thermo-oxidative stability is noticeably improved as indicated by the result from thermogravimetric analysis (TGA in air). Subsequently, 3-phenoxybenzoic acid (PBA) was polymerized in PPA with the pristine DND (1.0−30 wt %) in situ to generate *meta*-poly(ether−ketone)-grafted DND composites, *m*PEK-*g*-DND. It was found that the *m*PEK-*g*-DND nanocomposites were not only soluble in methanesulfonic acid (MSA), but also dispersed well in solvents such as *N*-methyl-2-pyrrolidinone (NMP) and tetrahydrofuran (THF). Their intrinsic viscosity values ranged from 0.67 to 1.42 dL/g in MSA at 30 °C. Interestingly, a polyelectrolyte effect was observed for the nanocomposites with DND content >10 wt %. As compared to the neat *m*PEK polymer, the glass transition temperatures of these nanocomposites were increased by as much as 19 °C, while their short-term thermal and thermo-oxidative stabilities, as defined by the temperatures at which 5 wt % loss ($T_{d5\%}$) occurred during TGA scans, were increased by 34−88 °C in air and 59−108 °C in nitrogen. The wide-angle X-ray diffraction results showed that the intensity of the characteristic diamond *d*-spacing (111) at 2.05 Å grew proportionately with the DND content in the samples. Morphological studies (SEM and TEM) provided further evidence to support the feasibility of polymer grafting and formation of in-situ nanocomposites.

Introduction

Although detonation nanodiamond (DND) was discovered relatively early (in the 1960s) in USSR[1] as compared to other carbon nanoparticles, viz. fullerenes, single-walled, double-walled, and multiwalled carbon nanotubes (SWNT, DWNT, and MWNT), and nanofibers (CNF), DND has received little or no attention until 1988 when two landmark papers appeared in the open literature.[2,3] Detonation nanodiamond was so named because of its production by detonation of 2,4,6-trinitrotoluene (TNT)/1,3,5-trinitrotriazacyclohexane (hexogen) explosives in a closed steel chamber either in gaseous atmosphere, e.g. CO_2 (dry method), or in water (wet method).[4] DND is also known by two other common names, viz. ultradispersed diamond (UDD) and ultrananocrystalline diamond (UNCD) particulates, because the basic constituents (primary nanoparticles) have the characteristic size in the range of 2−10 nm (average diameter ~ 4−5 nm) and very large specific surface area (≫200 m²/g).[5] With the important advantages such as availability in larger quantities (industrial production capabilities existing in Russia, Ukraine, China, and Belarus) and moderate cost, DND is very attractive as a material platform for nanotechnology. Further-

more, DND has been shown to be noncytotoxic and biocompatible.[6] These features give DND an additional appeal to bio-related applications in view of its rich surface chemistry that could be modified with relative ease.[7] The surface functional groups identified by various spectroscopic techniques are mostly oxygenated moieties such as −CO_2H (carboxylic acid), lactone, C═O (keto carbonyl), −C−O−C (ether), and −OH (hydroxyl),[4] and as such, the ND surfaces are very polar and hygroscopic. In addition, interparticle hydrogen bonding and formation of ester, ether, and anhydride bonds are believed to play important roles in assembling the DND primary particles into much larger aggregates with sizes ranging from a few hundred nanometers ("core agglutinates") to a few tens of microns ("agglomerates").[8] In fact, under appropriate pH conditions, these interparticle binding forces[9] are believed to be responsible for the large-scale self-assembly of acid-treated DND into fibers and thin films from drying the suspension.[10] Further, the primary particles in the core agglutinates are so strongly bound together that the total binding force is even greater than that in SWNT ropes, which stems from noncovalent (van deer Waals and π−π) interactions between individual nanotubes. Indeed, it is known that even powerful ultrasonication of crude nanodiamond aggregates could only produce core agglutinates with average size of 120 nm.[11]

Covalent surface modifications of diamond nanoparticles are generally focused on improving the DND processability and introducing suitable functional groups to impart, enhance, or

* Corresponding author: e-mail loon-seng.tan@wpafb.af.mil; Ph (937)255-9153; Fax (937)656-6327.
† University of Dayton Research Institute.
‡ AFRL/RXBN.
§ University of Dayton.
‖ Shinshu University.

tailor certain properties and, eventually, to increase system compatibility and performance. The synthetic tools for such modification have entailed the conversion of the oxygenated groups (i.e., carboxylic acid, hydroxyl, etc.) to suitable functionalities for subsequent manipulation. For example, DND was fluorinated using a F_2/H_2 mixture to afford 8.6 atom % fluorine (replacing OH, CO_2H, etc.) on the surface, and the fluorinated DND was then used as a precursor for the preparation of alkyl-, amino-, and acid-functionalized DNDs that showed an increased solubility in polar solvents and much smaller size in nanoparticle agglomeration[12] or coated covalently onto an amine-functionalized glass surface.[13] High-temperature (400−850 °C) treatment of DND powders in the presence of H_2, Cl_2, or NH_3 has also led to converting the surface carboxylic acid to alcohol, acid chloride, and nitrile, in that order.[14] More recently, the reduction of the surface $-CO_2H$ by the $BH_3 \cdot THF$ complex to the corresponding $-CH_2OH$, followed by O-silylation with (3-aminopropyl)trimethoxysilane and coupling with biotin or a short peptide to generate promising bio-nanohybrid materials, has been reported.[15]

Besides the aforementioned reports on the covalent functionalization of DND surfaces that were likely to have occurred at the outermost layer with mixed sp^2 and sp^3 carbons, Li et al. reported the first example of DND−polymer nanocomposites, in which poly(methyl methacrylate) brushes were grafted from initiators, previously and covalently bonded on the DND surface, by atom transfer radical polymerization (ATRP) process.[16] Most recently, Zhang et al. reported the grafting of aromatic polyimides from nanodiamonds.[17] In these reports, the DND component in the polymer nanocomposites was actually aggregates (20−50 nm) of primary particles, resulting in polymer−DND particles with sizes 100−200 nm.

Herein, we present for the first time *the possibility of polymer-grafting the primary nanodiamond particles* using an in-situ polymerization technique in polyphosphoric acid, which we believe is relatively effective in dispersing and sequestering the primary particles as well as promoting Friedel−Crafts (F−C) acylation in the grafting process. To our knowledge, there has been no work described on functionalization of DND via an electrophilic substitution reaction in solution state or similar grafting of polymers on the DND surface when this project was initiated.[18]

Experimental Section

Materials. Commercial DND agglutinates were subjected to stirred-media milling with 30 μm beads of zirconia in water. Clear, black, and stable 10% colloidal solution was obtained. More than 90 wt % of the deagglomerated DND was smaller than 8 nm as revealed by dynamic laser scattering measurements of particle-size distribution. Details of milling procedure have been described elsewhere.[19] As-received DND sample (black flakes) is consisting of somewhat hygroscopic, agglomerates of ∼4 nm primary particles. 4-(2,4,6-trimethylphenoxy)benzoic acid (TMPBA) was synthesized as previously reported.[20a] Commercially available (Aldrich Chemical Co.) AB monomer, 3-phenoxybenzoic acid (PBA), was recrystallized from heptane to give white needles (mp 146−147 °C). All other reagents and solvents were purchased from Aldrich Chemical Co. and used as received.

Instrumentation. Proton nuclear magnetic resonance spectra of polymer composites were measured at 300 MHz on a Bruker AVANCE 300 spectrometer. Infrared (IR) spectra were recorded on a Nicolet Nexus 470 Fourier transform spectrophotometer. Elemental analysis was performed by Systems Support Branch, Materials & Manufacturing Directorate, Air Force Research Laboratory, Dayton, OH. Intrinsic viscosities were determined with Cannon-Ubbelohde No. 150 viscometer. Flow times were recorded in methanesulfonic acid (MSA) solution, and polymer concentrations were approximately 0.5−0.10 g/dL at 30.0 ± 0.1 °C.

Differential scanning calorimetry (DSC) analysis were performed in nitrogen with a heating rate of 10 °C/min using a Perkin-Elmer DSC 7 thermal analyzer equipped with differential scanning calorimetry cell. Thermogravimetric analysis (TGA) was conducted in nitrogen (N_2) and air atmospheres at a heating rate of 10 °C/min using a TA Hi-Res TGA 2950 thermogravimetric analyzer. The scanning electron microscope (SEM) and transmission electron microscope (TEM) used in this work were a Hitachi S-5200 and Hitachi H-7600, respectively. TEM sample preparation: the 10 wt % *m*PEK-*g*-DND sample (∼2 mg) was dissolved in DMF (∼2 mL) and sonicated for a few minutes. Then, a TEM grid was dipped into the resulting *m*PEK-*g*-DND/DMF solution, lifted up, and let dry in air, followed by drying on a hot plate (preheated to ∼60−80 °C) for a few minutes. The TEM was operated at 100 keV. Wide-angle X-ray diffractions (WAXS) of compression-molded samples were recorded with a Rigaku RU-200 diffractometer using Ni-filtered Cu KR radiation (40 kV, 100 mA, $\lambda = 0.154\ 18$ nm).

Functionalization of DND with 4-(2,4,6-Trimethylphenoxy)benzoic Acid (3, TMPB-*g*-DND). Into a 100 mL resin flask equipped with a high-torque mechanical stirrer, and adaptors for nitrogen inlet and outlet, TMPBA (0.20 g, 0.78 mmol), DND (0.20 g), PPA (83% P_2O_5 assay, 10 g), and phosphorus pentoxide (P_2O_5, 2.5 g) were charged, and the reaction mixture was stirred under dried nitrogen purging at 130 °C for 72 h. After cooling down to room temperature, water was added to the reaction mixture. The resulting precipitate was collected, washed with diluted ammonium hydroxide, and Soxhlet extracted with water for 3 days and methanol for 3 days. It was then dried over P_2O_5 under reduced pressure at 100 °C for 72 h to afford 0.31 g (80% yield) of gray solid. Anal. Calcd for $C_{7.89}H_3N_{1.75}O_{0.56}$ (based on the assumption that for every 100 carbons there are 2.35 4-(2,4,6-trimethylphenoxy)benzoyl groups attached): C, 87.58%; H, 2.10%; N, 1.75%; O, 7.01%. Found: C, 86.73%; H, 1.58%; N, 1.90%; O, 7.51%. ^{1}H NMR (DMSO-d_6, δ in ppm): 2.03 (s, 6H), 2.27 (s, 3H), 6.88 (d, 2H), 7.001 (s, 2H), 7.69 (d, 2H). FT-IR (KBr, cm^{-1}): 3418 (OH), 2922 (CH_3), 1712 (O−C=O), 1658 (C−C=O), 1595, 1234, 1157, 1079.

PPA-Treated DND (4, PT-DND). Product **4** was prepared from DND (0.20 g), PPA (83% P_2O_5 assay, 20 g), and phosphorus pentoxide (P_2O_5, 5.0 g) using the same procedure used for compound **3** to afford 0.18 (90% yield) of a black solid. Anal. Found: C, 90.87%; H, 1.10%; N, 1.92%; O, 4.98%. FT-IR (KBr, cm^{-1}): 3421, 2921, 1717, 1627, 1259, 1083, 990.

Representative Procedure for in-Situ Polymerization (6f, *m*PEK with 20 wt % DND Load). Into a 250 mL resin flask equipped with a high-torque mechanical stirrer, adaptors for nitrogen inlet/outlet, and a solid-addition port, PBA (4.00 g, 18.7 mmol), DND (1.00 g), and PPA (83% P_2O_5 assay; 100 g) were placed, and the reaction mixture was stirred under dry nitrogen purge at 130 °C for 3 h. P_2O_5 (25.0 g) was then added in one portion via the solid-addition port. The initially dark mixture (due to dispersion of DND) became lighter in color and more viscous as the polymerization of PBA and the growth of *m*PEK grafts progressed. The temperature was maintained at 130 °C for 48 h. At the end of the reaction, the color of mixture was dark brown, and upon addition of water, purple solids precipitated. The resulting purple nanocomposite clusters were put into a Waring blender, and the solid chunks were chopped, collected by suction filtration, and washed with diluted ammonium hydroxide. Then, the nanocomposite product was Soxhlet-extracted with water for 3 days and then with methanol for 3 more days and was finally dried over phosphorus pentoxide under reduced pressure at 100 °C for 72 h to give a purple powder in quantitative yield. Anal. Calcd for $C_{6.84}H_{3.44}N_{0.03}O_{0.44}$: C, 82.20%; H, 3.44%; N, 0.44%; O, 13.92%. Found: C, 81.44%; H, 3.57%; N, 0.21%; O, 12.74%. FT-IR (KBr; cm^{-1}): 3431, 3063, 1657 (carbonyl), 1576, 1433, 1237, 1161, 877, 757.

Extraction of Free *m*PEK from 20 wt % *m*PEK-*g*-DND, 6f. The AB monomer (3-phenoxybenzoic acid) is soluble in hot methanol, but the derived polymer, *m*PEK, is not. However, *m*PEK is very soluble in methylene chloride (CH_2Cl_2). Therefore, **6f** (purple powder sample, 1.00 g) was dispersed in CH_2Cl_2 in a closed vial

at room temperature for 48 h. During this period, the suspension was sonicated followed by filtration through 0.2 µm PTFE membrane. The purple solid was collected. It was dispersed in fresh CH_2Cl_2, sonicated, and filtered again. Filtrate was spotted on a thin-layer chromatography (TLC) plate and checked for fluorescence due to *m*PEK with a hand-held UV lamp. The above extraction routine was repeated three times until TLC showed no sign (fluorescent spot) of free *m*PEK in the CH_2Cl_2 filtrate. After the removal of CH_2Cl_2 from the sample, the residue was dried in vacuum to afford 0.92 g of purple powder. This test indicates that most of *m*PEK has been grafted onto DND.

Friedel−Crafts Acylation of Adamantane with 2,4,6-Trimethylphenoxybenzoic Acid (8). The synthesis of compound **8** was attempted from a mixture of adamantane (0.50 g, 3.7 mmol), TMPBA (1.0 g, 3.9 mmol), PPA (83% P_2O_5 assay, 100 g), and phosphorus pentoxide (P_2O_5, 25.0 g) using the same procedure used for compound **3**. After similar work-up, the two starting materials were recovered quantitatively, and no Friedel−Crafts product **8** [4-(2,4,6-trimethylbenzoylphenoxy)benzoyl]-1-adamantane was detected based on mass spectra, FT-IR, and NMR results.
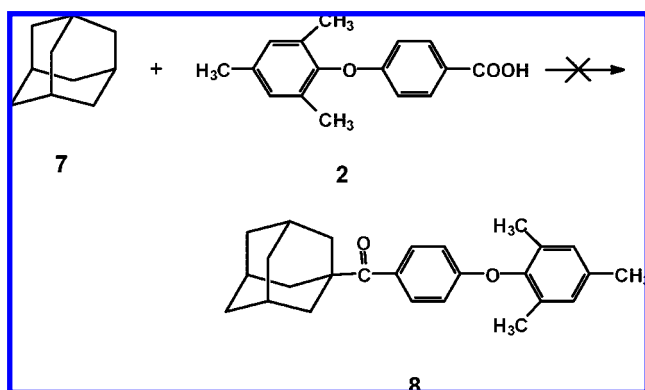
Results and Discussion

Previously, on the basis of model-compound studies, we have reported that Friedel−Crafts (F−C) acylation in polyphosphoric acid (PPA) is a viable, alternative route to effecting a controlled covalent functionalization of VGCNF and MWNT.[20] VGCNF and MWNT were not only functionalized with TMPBA as a model for F−C acylation in PPA but were also grafted when they were in attendance during the polymerization of the respective AB and AB_2 monomers in PPA using the optimized conditions that we have described[21] to generate linear *m*PEK and hyperbranched-PEK nanocomposites. Because of the significant hydrogen content in the starting VGCNF and MWNT, we concluded that the covalent attachment of the arylcarbonyl groups most probably had occurred at the sp^2 C−H defect sites.

Model Reaction of DND with TMPBA (2). As noted by Ōsawa et al.,[19] DNDs have never been isolated in pure form (>99.9% carbon). Elemental analysis of the pristine DND has revealed significant presence of heteroatoms (H, N, O) in addition to carbon (Table 1). The carbon content is only 90.35% instead of theoretical value of 100% in a pure diamond. However, the diamond content (77%) of DND is even lower than natural diamond (99.42%).[19] Therefore, an isolated diamond nanoparticle may be considered as having a central diamond (sp^3 C) core surrounded by an outer shell comprising of a mixture of sp^2 and sp^3 carbons.[22] It is conceivable that a hydrogenated surface or a fullerenic outer shell ("Bucky diamond") may also exist.[23−25] However, the surface composition and chemistry of this outer layer would have significantly changed upon typical postproduction treatment of the raw DND with nitric and sulfuric acids. Osswald et al. reported that their DND samples contained 19−30% of sp^2 carbons after oxidizing-acid (H_2SO_4 and HNO_3) treatment of raw DND, which contained

Table 1. Elemental Analysis Data for Pristine DND, TMPB-*g*-DND, PT-*g*-DND, and *m*PEK-*g*-DND

sample	elemental analysis	C (%)	H (%)	N (%)	O (%)
pristine DND	calcd	100	0	0	0
	found[a]	90.35	1.06	2.06	4.87
TMPB-*g*-DND	calcd[b]	87.58	2.10	1.75	7.01
	found	86.73	1.58	1.90	7.51
PT-DND	calcd	100	0	0	0
	found	90.87	1.10	1.92	4.98
*m*PEK-*g*-DND, 1 wt %	calcd[c]	79.74	4.05	0.02	16.19
	found	79.43	4.33	<0.1	15.87
*m*PEK-*g*-DND, 2 wt %	calcd[c]	79.82	4.01	0.04	16.06
	found	79.18	4.21	<0.1	15.67
*m*PEK-*g*-DND, 5 wt %	calcd[c]	80.25	3.92	0.11	15.71
	found	80.07	3.92	0.08	15.67
*m*PEK-*g*-DND, 10 wt %	calcd[c]	80.41	4.26	0.21	15.12
	found	80.69	3.84	0.16	14.93
*m*PEK-*g*-DND, 20 wt %	calcd[c]	82.20	3.44	0.44	13.92
	found	81.44	3.57	0.21	12.74
*m*PEK-*g*-DND, 30 wt %	calcd[c]	83.47	3.14	0.66	12.73
	found	83.53	3.14	0.61	12.48

[a] Based on the elemental analysis result, the empirical formula of pristine DND is $C_{7.52}H_{1.06}N_{0.15}O_{0.30}$, which was used in the subsequent calculation of *m*PEK-*g*-DND nanocomposites compositions. [b] TMPB-*g*-DND's molecular formula of $C_{7.89}H_3N_{1.75}O_{0.56}$ is based on the assumption that for every 100 carbons there are 2.35 4-(2,4,6-trimethylphenoxy)benzoyl groups attached. The molecular formula of 4-(2,4,6-trimethylphenoxy)benzoyl group is $C_{16}H_{15}O_2$. [c] Calculated composition based on the assumption that the molar mass of the repeat unit of *m*PEK, $C_{13}H_8O_2$, is 196.20. Empirical formulas derived from the molar ratios of DND:*m*PEK, i.e., C: $C_{13}H_8O_2$, are as follows: (1/99) $C_{6.64}H_{4.05}N_{0.0016}O_{1.01}$; (2/98) $C_{6.65}H_{4.01}N_{0.003}O_{1.00}$; (5/95) $C_{6.67}H_{3.92}N_{0.008}O_{0.98}$; (10/90) $C_{6.70}H_{4.22}N_{0.015}O_{0.95}$; (20/80) $C_{6.84}H_{3.44}N_{0.03}O_{0.44}$; (30/70) $C_{6.91}H_{3.12}N_{0.05}O_{0.79}$.

77% of sp^2 carbons.[26] DND used in this work contains 1.06% of hydrogen, which is comparable to that of the acid-treated nanodiamond reported. On the basis of the information on the sp^2 and sp^3 C−H contents and the sp^2/sp^3 carbon ratios of various grades of DND samples in ref 26, we estimate that DND at most contains 2.7−4.2 atom % of sp^2 C−H defects, which would be susceptible to a Friedel−Crafts acylation in PPA/P_2O_5 medium.[27]

Although in colloidal solution the primary DND particles are 2−6 nm in diameter, they readily self-organize, upon solvent removal, into clusters or primary aggregates (20−30 nm), which in turn form larger but weakly bonded secondary aggregates in a broad size distribution, ranging from hundreds of nanometers to a few micrometers sizes, as shown in SEM images (Figures 1a,b). This agglomeration observed in solid state is driven by the surface functional groups with high polarity and strong H-bonding capability, such as COOH, OH etc., which were created along with the other functionalities by postsynthesis, acid treatment to purify raw DND.[28] Thus, to disperse the DND quickly into PPA during the reaction, the pristine DND powder was gently ground to particulate with sizes of 20−30 nm using a spatula (Figures 1c,d). Subsequently, the ground DND (**1**) was treated with TMPBA (**2**) in PPA/ P_2O_5 at 130 °C for 72 h (Scheme 1). After the reaction mixture had been precipitated in water, the crude product (**3**) was washed with water, treated with aqueous ammonium hydroxide to neutralize the residual phosphoric acid, and finally subjected to an extensive Soxhlet extraction with water and methanol to completely remove the residual phosphoric acid and any unreacted **2**. The resulting product designated as TMPB-*g*-DND (**3**) was finally dried under reduced pressure at 100 °C for 72 h.

Characterization of TMPB-*g*-DND (3). The FTIR spectrum of a pristine DND/KBr pellet (Figure 2a) shows a strong, broad absorption band centered at 3421 cm^{-1}, attributable to the O−H stretching bands of the DND-bound hydroxyl and carboxylic acid moieties and possibly difficult-to-remove, residual H_2O in KBr lattice. The somewhat asymmetric shape of this OH band
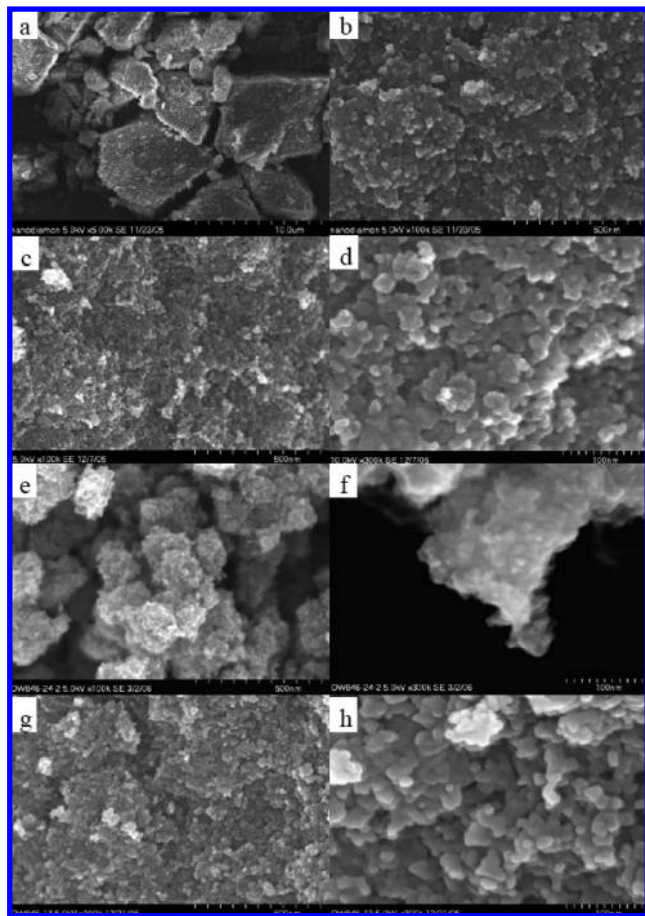
Figure 1. SEM images of (a) pristine DND (×5K), (b) pristine DND (×100K), (c) pristine (spatula-ground) DND (×100K), (d) pristine (spatula-ground) DND (×300K), (e) TMPB-*g*-DND (×100K), (f) TMPB-*g*-DND (×300K), (g) PT-DND (×100K), and (h) PT-DND (×300K). Scale bar for (a) is 10 μm. Scale bars for (b), (c), (e) and (g) are 500 nm. Scale bars for (d), (f) and (h) are 100 nm.

that extends to around 2000 cm^{-1} is also quite interesting. This feature was also present for PPA-treated DND, but it practically disappeared in TMPB-*g*-DND (see the enlargement of this spectral region in Figure 2). [We propose that this is an indication of intermolecular (interparticle) hydrogen bonding involving OH groups in DND.] The aromatic $\nu(sp^2$ C−H) peak is typically very weak in the 3000−3200 cm^{-1} region and possibly hidden underneath the broad $\nu(OH)$ band. The small peak around 2921 cm^{-1} is attributed to aliphatic sp^3 C−H. The bands at 1717 and 1627 cm^{-1} are assigned to the carbonyl (C=O) stretching mode of carboxylic acid and the OH bending mode, respectively. After DND has been treated with compound **2** under Friedel−Crafts acylation conditions, TMPB-*g*-DND shows the expected doubly conjugated ketone $\nu(CO)$ band at 1658 cm^{-1} as well as the characteristic stretches assignable to Ar−O−Ar linkage (1232 cm^{-1}). The increased intensity at 2923 cm^{-1} is due to the three methyl groups of the aryl ketone pendant (Figure 2b). It seems that the absorption band of carboxylic acid around 1717 cm^{-1} remained more or less intact, shifted slightly to 1712 cm^{-1}. Thus, FT-IR results indicate that the sp^2 C−H moieties are indeed present on the DND surface and accessible for Friedel−Crafts acylation. The sp^3 C−H bonds on DND surface are not expected to be reactive, and it is confirmed by the lack of reaction of adamantane with TMPBA in PPA under the same reaction conditions.

On the basis of the elemental analysis results of DND and TMPB-*g*-DND, it can be deduced that there are ∼2.3 arylcarbonyl groups covalently attached to the nanodiamond structure

for every 100 carbon sites (see Table 1 and the associated footnotes). This value (2.3 atom %) is at the low end of calculated sp^2 C−H defects, i.e., 2.7−4.2 atom % (vide supra).

Figure 3 shows, for comparison purposes, the composite TGA behaviors (in air and nitrogen) of the pristine DND and the functionalized DND, **3**. In a nitrogen atmosphere, all three samples, pristine DND, TMPD-*g*-DND, and PT-DND, behave more or less the same, but in air, their TGA behaviors are distinctly different.

In air, the unmodified DND suffered 1.5% weight loss around 300 °C, followed by 1.7% of weight gain at 480 °C. The early weight loss is due to the absorbed moisture and other unknown volatiles in DND. The weight gain, peaking at 480 °C, is most probably due to the oxidation of some sp^2 carbons on DND surface to form oxygenated moieties, which may be lost as CO/CO$_2$ at higher temperatures.[29] Finally, DND commenced a catastrophic weight loss at 500 °C, but it lost only 7.4% of its weight at 850 °C in nitrogen.

Unlike similarly functionalized VGCNF and MWNT, which have shown a distinct two-stage degradation profile,[20] TMPB-*g*-DND displays a continuous degradation pattern primarily due to the overlap of the degradation temperatures of DND and TMPB pendants. Thus, the degree of functionalization could not be estimated by the TGA method. However, despite that TMPB-*g*-DND started to lose weight at a lower temperature (∼400 °C), it surpassed the pristine DND in the thermo-oxidative stability at temperatures ≥600 °C. Similar enhancement in thermo-oxidative stability is also observed for PT-DND (vide infra). Thus, the fact that similar enhancement of thermo-oxidative stability during the TGA runs in air was also recorded for VGCNF and MWNT, which had been treated with PPA/P$_2$O$_5$ at 130 °C or functionalized with TMPB, appears to hint at the possibility of some structural similarity among VGCNF, MWNT, and DND.

The morphology of DND changed dramatically after functionalization. An immediate impression is that TMPB-*g*-DND in the solid state consisted of agglomerates ∼200 nm (Figure 1e), which are larger than those of spatula-ground, pristine DND (primary aggregate with average diameter ∼20−30 nm) (Figures 1c,d). In addition, the fuzziness of the magnified image shows that the primary particles (∼10 nm) of TMPB-*g*-DND seem to have been shrouded behind a veil of organic constituents (Figure 1f). Since the surface functional groups would play a pivotal role in determining the morphology and properties of DND in the bulk state, we speculate that after DND has been functionalized, and in solid state, the surface-tethered TMPB groups must have played a role in driving the formation of larger clusters (i.e., ∼200 nm agglomerates), most probably via the $\pi-\pi$ interactions involving the planar, electron-donating 2,4,6-trimethylphenoxy component of TMPB.

Solution Properties. TMPB-*g*-DND could be almost instantaneously dispersed in common organic solvents, such as *N*-methylpyrrolidinone (NMP), dimethyl sulfoxide (DMSO), tetrahydrofuran (THF), methylene chloride, and methanesulfonic acid (MSA) upon sonication, while the pristine DND could be dispersed only in DMSO, water, or ethanol. For example, both TMPB-*g*-DND and pristine DND formed suspension solution in THF right after sonication. However, the pristine DND "precipitated" out of THF in 2 h while TMPB-*g*-DND remained homogenously dispersed in solution for weeks (see Figure SS-1 in the Supporting Information). TMPBA and pristine DND exhibit UV absorption peaks at 264 and 265 nm, respectively (see Figure SS-2, Supporting Information). After functionalization, the absorption maximum of TMPB-*g*-DND was red-shifted to 277 nm. While no peak shifting was observed for simple physical adsorption of cytochrome on nanodiamond,[30] the red shift of TMPB-*g*-DND provides another piece of positive

Scheme 1. Synthesis of TMPB-*g*-DND[a]
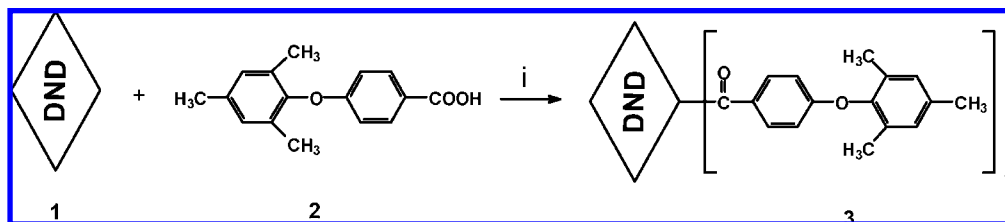
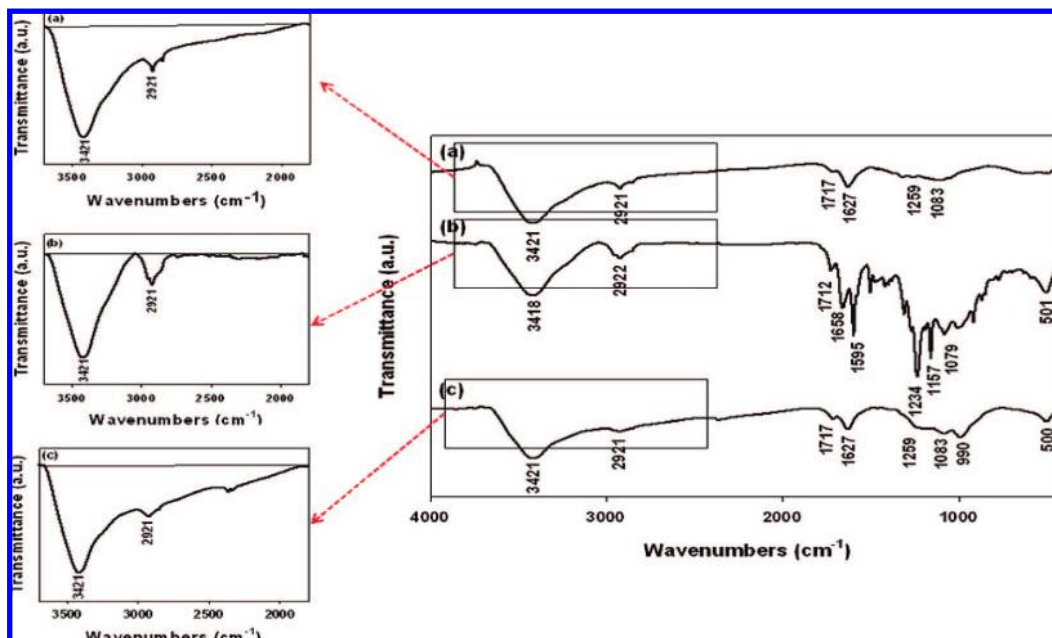[a] (i) PPA/P$_2$O$_5$, 130 °C. The product structure is idealized.

Figure 2. FT-IR spectra: (a) pristine DND, (b) TMPB-*g*-DND, and (c) PT-DND. From the enlargement of this spectral region (left side of the figure), both pristine-DND and PT-DND clearly depict their ν(OH) bands to be more asymmetric and much broader than that of TMPB-*g*-DND, whose bulky TMPB groups on the surface would have likely retarded interparticle hydrogen bonding.
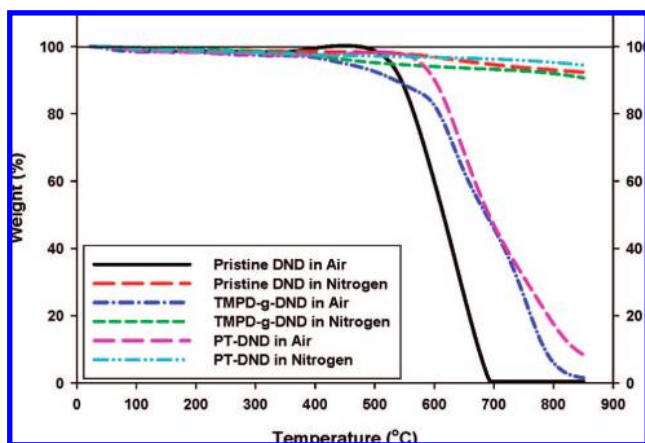

Figure 3. TGA thermograms of pristine DND, TMPB-*g*-DND, and PT-DND in air and nitrogen, at a heating rate of 10 °C/min.

evidence for a successful functionalization. In the UV−vis spectra, the baselines (for example, from 300 to 800 nm) increase for DND and TMPB-*g*-DND in comparison to TMPBA are most probably due to the absorption of the fullerenic part of DND surface.

Proton NMR characterization of TMPB-*g*-DND in solution was also conducted. The discussion of the result will be more meaningful together with that of *m*PEK-*g*-DND nanocomposite sample (vide infra).

Table 2. Thermal Stability of Pristine DND, TMPB-*g*-DND, and PT-DND

sample	in nitrogen		in air	
	$T_{d5\%}$[a] (°C)	char[b] (%)	$T_{d5\%}$[a] (°C)	char[b] (%)
pristine DND	681	92.4	527	0.48
TMPB-*g*-DND	515	90.7	449	1.59
PT-DND	820	94.5	577	8.42

[a] Temperature at which 5% weight loss recorded on TGA thermogram run at a heating rate of 10 °C/min. [b] Char yield at 850 °C.

PPA-Treated DND. In order to investigate the effect of PPA/P$_2$O$_5$ on DND, we conducted a control experiment, in which DND alone was heated in PPA/P$_2$O$_5$ at 130 °C for 3 days to afford a sample, designated as PT-DND, in 90% recovery yield. The work-up procedure was same as that for TMPB-*g*-DND. The IR spectrum of PT-DND is essentially identical with that of the pristine DND, except that most of the absorption peaks of PT-DND are sharper (Figure 2c). The TGA results indicate that the thermo-oxidative stability of PT-DND has been significantly improved over the pristine DND (Figure 3c). The powder samples PT-DND shows a 5% weight loss at 577 °C, 50 °C higher than the pristine DND, in air. PT-DND was also observed to generate a higher char yield (94.5%) than the pristine DND (92.4%) in nitrogen (Table 2). The higher stability of PT-DND is probably due to the removal of some inorganic impurities from the pristine DND during PPA treatment. The sizes and shapes (Figures 1g,h) of PT-DND are similar to the ground pristine DND shown in Figure 1, albeit the surface of

Scheme 2. In-Situ Polymerization of 3-Phenoxybenzoic Acid with DND[a]

DND, %	0	1.0	2.0	5.0	10	20	30
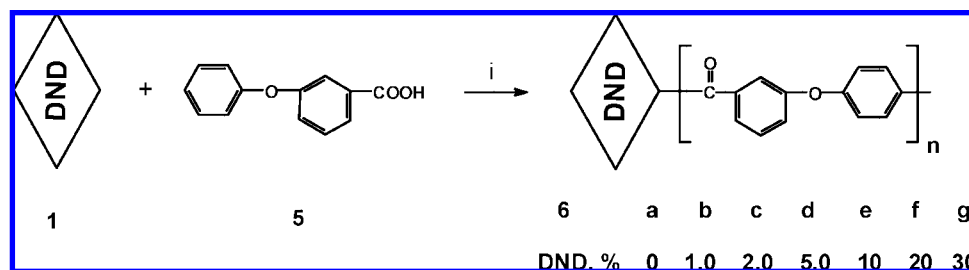
[a] (i) PPA/P_2O_5, 130 °C.

Table 3. Physical Properties of *m*PEK-*g*-DND Composites

		DSC			TGA			
		first heating		second heating	in nitrogen		in air	
DND (wt %)	$[\eta]^a$ (dL/g)	T_{exo}^b (°C)	ΔH (J/g)	T_g^c (°C)	$T_{d5\%}^d$ (°C)	char^e (%)	$T_{d5\%}^d$ (°C)	char^e (%)
0	0.46	136 (T_g)		136	402	47.1	414	0.80
1.0	0.67	131	2.64	138	461	46.8	448	1.18
2.0	0.88	132	3.78	138	478	49.0	452	1.56
5.0	1.03	134	6.3	139	467	50.3	463	1.56
10	1.42	137	7.8	143	501	54.1	489	1.78
20	1.37	143	6.5	151	488	58.6	498	1.14
30	0.95	147	5.9	154	510	62.5	502	0.42

[a] Intrinsic viscosity measured in MSA at 30.0 ± 0.1 °C. [b] Exothermic peak on DSC thermogram obtained in N_2 with a heating rate of 10 °C/min. [c] Inflection in baseline on DSC thermogram obtained in N_2 with a heating rate of 10 °C/min. [d] Temperature at which 5% weight loss recorded on TGA thermogram run at a heating rate of 10 °C/min. [e] Char yield at 850 °C.

PT-DND has become slightly smoother. All the above results indicate that, apart from being an efficient Friedel–Crafts catalyst, PPA is also chemically benign to the DND structure and improves the thermal stability of DND by effectively removing the residual contaminants.

In-Situ Polymerization and Characterization of DND/*m*PEK Nanocomposites. In our previous work, linear and hyperbranched PEKs have been grafted onto the surface of either MWNT or VGCNF (both as-received) in PPA with optimized P_2O_5 content, resulting in uniform grafting ether–ketone polymers to these carbon nanoscale materials.[20] In this work, an in-situ polymerization of PBA in the presence of dispersed DND was carried out with different PBA:DND ratios as shown in Scheme 2, and the results are summarized in Table 3. The initial color of the reaction mixture was gray because of the DND dispersion. As the reaction continued at the polymerization temperature, the color of the reaction mixture changed from gray to dark brown. Also, as the amount of DND was increased in the polymerization mixtures ("dopes"), the dope stuck to the stirring rod sooner, and the bulk viscosity increased dramatically. After the polymerization process had been terminated, the dope was precipitated into water and collected by filtration. Both water and methanol was used successively in Soxhlet extraction to remove residual phosphoric acid and *m*PEK oligomers. The color of the resulting *m*PEK-*g*-DND powder is deep purple, in contrast to the pink color for *m*PEK and black color for *m*PEK-*g*-VGCNF (see TOC graphic and Figure SS-3 in Supporting Information). Since DND powder is black, the purple *m*PEK-*g*-DND indicates a better dispersion of DND in *m*PEK than *m*PEK-*g*-VGCNF, resulting in the color dominance by *m*PEK over DND. The FT-IR spectrum of 20 wt % *m*PEK-*g*-DND (Figure 4c) depicts practically all the IR bands that match those for the pure *m*PEK (Figure 4b). The element contents of the nanocomposites were calculated based on the feed ratios of the pristine DND and monomer.[20b] The calculated values show good agreement with the elemental analysis data (Table 1).

Finally, since the main objective of this work is to prepare *m*PEK-*g*-DND nanocomposites in a one-pot fashion, a system-atic effort to determine the presence of free *m*PEK in them was not undertaken. However, from a simple extraction-and-weighing experiment on one of the samples (20 wt % *m*PEK-*g*-DND; see Experimental Section for details), we estimated ∼8 wt % or less of free *m*PEK in the nanocomposites.

Solution Properties of *m*PEK-*g*-DND. The resulting in-situ nanocomposites are slightly soluble in NMP and methylene chloride, in which *m*PEK dissolves easily, but in a visual sense, they dissolve readily in MSA to form clear and homogeneous solutions. After their MSA solutions had been filtered through glass filters (practically there were no residues visually detectable on the filters), the filtrates were used to measure the reduced and inherent viscosities of the nanocomposites. Both viscosities were plotted versus the solution concentration as shown in Figure 5. When the DND contents are ≤10 wt %, both reduced and inherent viscosities behave linearly as a function of concentration; i.e., no polyelectrolyte effect was observed. The intrinsic viscosities were determined from the extrapolation of reduced and inherent viscosities to zero concentration (Table 3). However, the reduced viscosity and inherent viscosities of 20 and 30 wt % *m*PEK-*g*-DND increased rapidly at diluted concentration (>0.2 g/dL), which indicates that the solution has a polyelectrolyte effect, which was not observed at lower concentrations (≤10 wt %). While we are not quite certain about the origin of this polyelectrolyte effect, we speculate that the electrostatic nature[9] of DND surface may play a role here by exerting its effect as the polymer grafts are shorter at higher DND contents. Nevertheless, the intrinsic viscosities were determined approximately from the two-point (30 wt %) or three-point (20 wt %) extrapolation of reduced and inherent viscosities to zero concentration (Table 3). All *m*PEK-*g*-DND composites display much higher viscosities (0.67–1.42 dL/g) than the neat polymer, which shows a viscosity of 0.46 dL/g at 30 °C in MSA (Table 3).

Nuclear Magnetic Resonance (NMR). Although DND can be dispersed into DMSO to form a homogeneous suspension, no peak was detected in its ^{1}H spectrum (Figure 6a). After DND
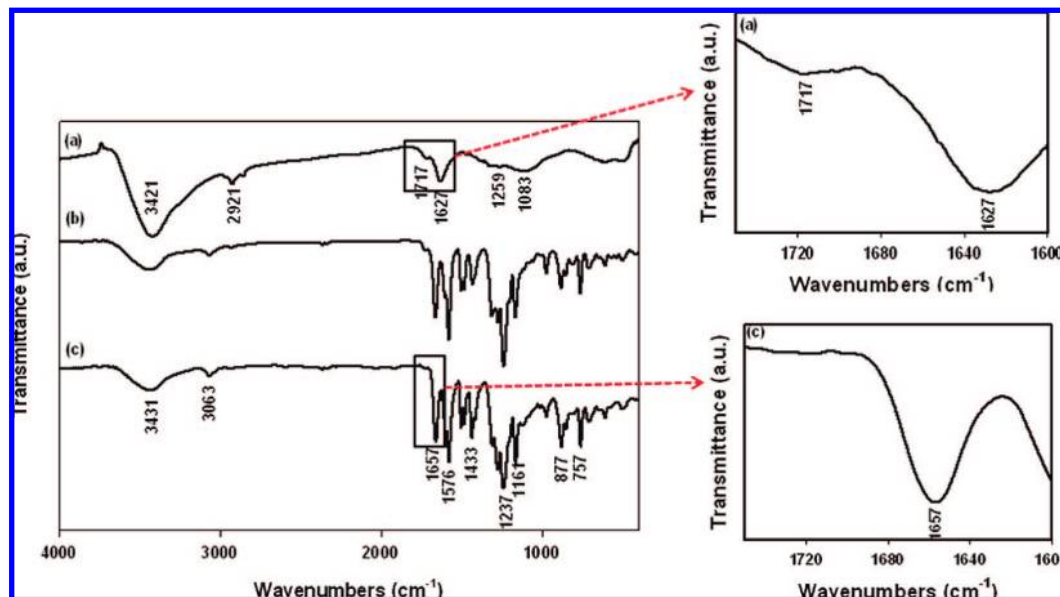
Figure 4. FT-IR spectra: (a) pristine DND, (b) *m*PEK, and (c) *m*PEK-*g*-DND, 20 wt %. In enlarging the spectral regions as indicated by arrows (right side of the figure) for pristine DND and *m*PEK-*g*-DND, it clearly shows the disappearance of the carboxylic acid *ν*(CO) at 1717 cm⁻¹. This implicates the participation of DND-bound COOH groups as grafting sites for Friedel−Crafts polymerization of 3-phenoxybenzoic acid in PPA.
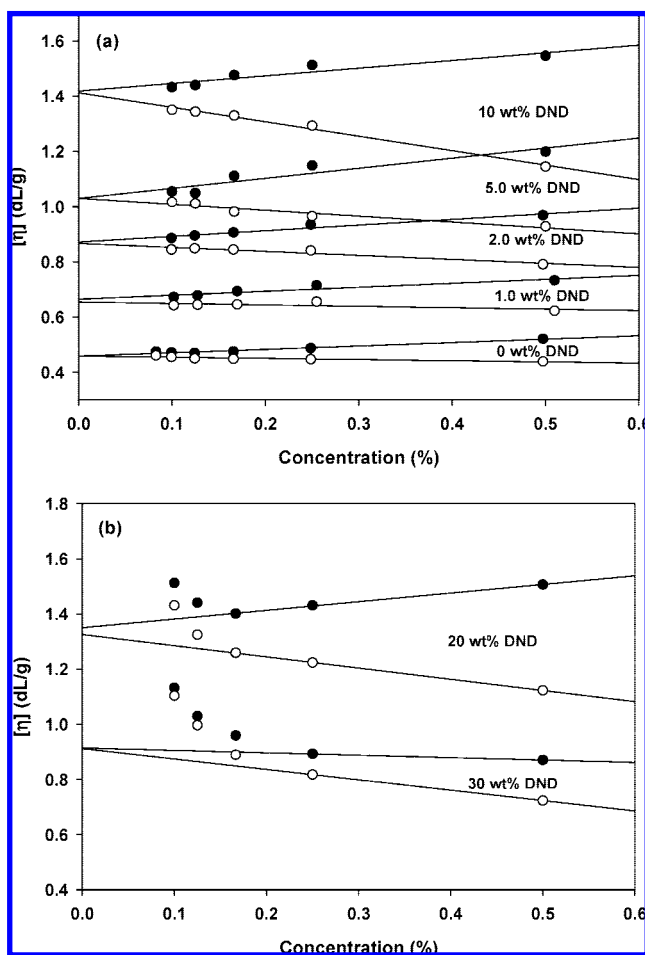

Figure 5. Solution viscosity vs concentration plots of *m*PEK-*g*-DND in methanesulfonic acid.

had been grafted with TMPB groups, the proton resonances of the resulting TMPB-*g*-DND were shifted accordingly. The resonance due to the aromatic C−H ortho to the carbonyl group changed from 7.91 ppm in TMPDA to 7.69 ppm in TMPB-*g*-DND, but the resonance due to the aromatic C−H ortho to ether
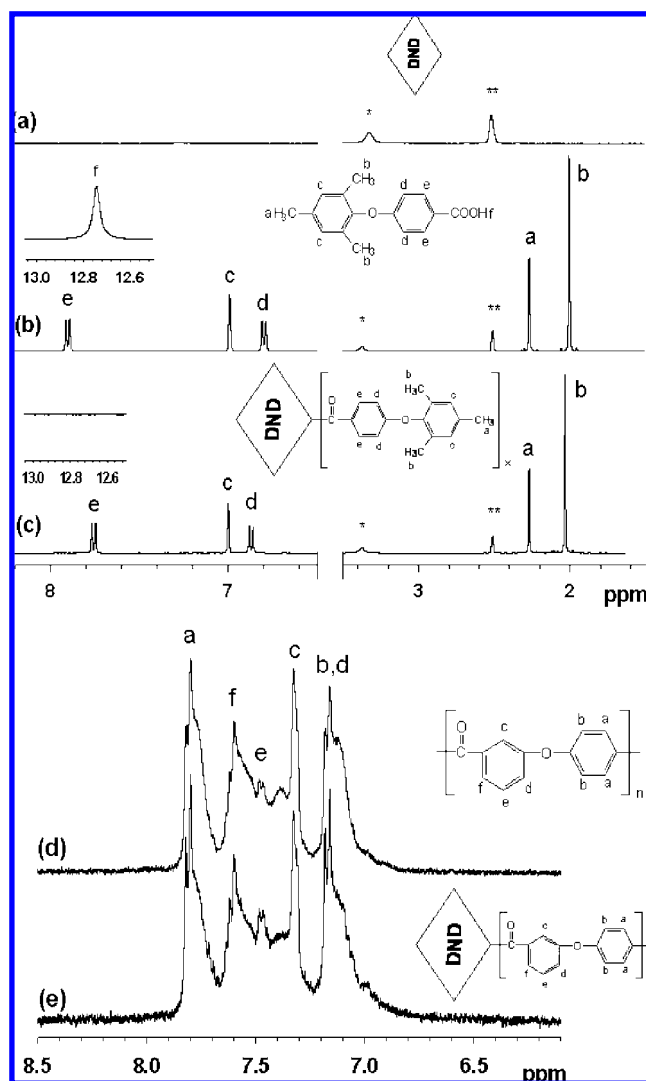

Figure 6. NMR spectra of (a) DND, (b) TMPBA, (c) TMPB-*g*-DND, (d) *m*PEK, and (e) *m*PEK-*g*-DND, 20 wt %. Signals due to proton impurities are marked by * for water and ** for DMSO.
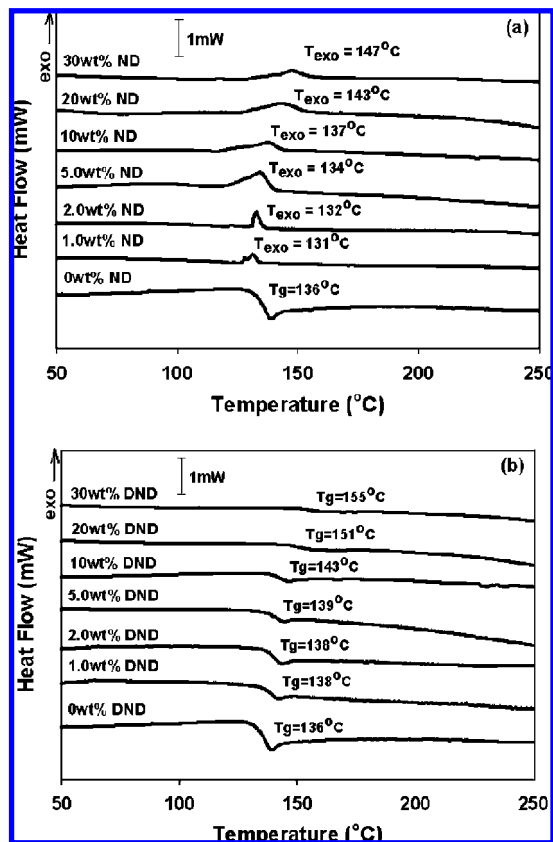
Figure 7. DSC thermograms of *m*PEK-*g*-DND samples run at a heating rate of 10 °C/min under nitrogen: (a) initial scan from room temperature; (b) rescan after cooling to room temperature.

linkage was increased from 6.76 ppm in TMPDA to 6.86 ppm in TMPD-*g*-DND. The O−H resonance of carboxylic acid observed for TMPBA was absent in TMPB-*g*-DND. All these observations indicated a successful grafting of 4-(2,4,6-tri-methylphenoxy)benzoyl groups onto DND. The proton signals of methyl groups were almost the same before and after grafting (Figures 6b,c). ^{1}H NMR spectra of *m*PEK and *m*PEK-*g*-DND are shown in Figures 6d,e. Resonances observed at 7.12, 7.18, 7.32, 7.48, 7.62, and 7.82 ppm for the nanocomposite are readily assigned to the corresponding resonances of the neat polymer. Unlike the considerable signal broadening which has been observed after the organic moieties had been grafted onto carbon nanotubes,[31] very little relaxation broadening was observed for TMPB-*g*-DND and *m*PEK-*g*-DND. Similar results were reported by Li et al. after poly(isobutyl methylate) brush had been grafted onto nanodiamond particles via ATRP.[16]

Thermal Properties. The glass-transition temperatures (T_g's) and exotherms of *m*PEK-*g*-DND samples were determined by DSC. The powder samples were heated to 300 °C in the DSC chamber in the first run and cooled to ambient temperature at 10 °C/min under nitrogen purge. Then, the samples were heated to 300 at 10 °C/min in the second run. As shown in Figure 7 and data summarized in Table 3, pure *m*PEK displays a T_g at 136 °C during both first and second heating runs. However, the *m*PEK-*g*-DND samples show exotherms with peak values varying between 131 and 147 °C, and no T_g's were detected during the first heating runs. The exothermic peak value increases somewhat proportionately with DND contents. The exotherms of as-produced samples (i.e., without prior heat treatment to 300 °C) were attributed to the storage strain energy induced by the shear field (i.e., generated by mechanically stirring) during the polymerization process at 130 °C in viscous PPA.[32] After polymerization, the samples were cooled down

and the storage strain energy of *m*PEK was retained kinetically by the increase in PPA bulk viscosity. When they were heated close to T_g's, the frozen polymer chains started to move, with the strain energy being released. For neat *m*PEK, no exotherm was observed during the first heating run. Since its T_g at 136 °C is very close to polymerization temperature (130 °C), either the storage strain energy did not build up or it was released just before cooling down due to its lower viscosity than *m*PEK-*g*-DND after polymerization. The T_g's of the nanocomposites appear in the second heating scan. As the amount of DND increased, the T_g's of the nanocomposites gradually increased to 155 °C for 30 wt %. This is consistent with the rationale that the attachment of flexible *m*PEK chains to the rigid DND surface imposes constraints over their mobility, resulting in as much as a 19 °C increase in the glass-transition temperature. In short, the presence of a single T_g for all the *m*PEK-*g*-DND samples, which increases monotonously with an increase in DND content, provides a strong support to the assertion that the polymer-grafted diamond nanoparticles were indeed homogeneously dispersed throughout the nanocomposites and the effectiveness of our in-situ polymerization method.

All the nanocomposites could be easily moldable at temperatures around 130 °C into tough sample bars with varied optical quality. For example, the sample bars containing 10 wt % DND are transparent and the ones containing 20 wt % DND are translucent (Figure SS-4, Supporting Information).

The TGA experiments on the powder sample of pure DND indicated that the temperatures at which 5% weight loss ($T_{d5\%}$) occurred were at 527 °C in air and 681 °C in nitrogen. On the other hand, the $T_{d5\%}$ values of pure *m*PEK were much lower, about 414 °C in air and 402 °C in nitrogen. The thermal stability of *m*PEK increased dramatically after it had been grafted onto DND surface. The $T_{d5\%}$ of *m*PEK-*g*-DND containing 1.0 wt % of DND increased from 414 to 448 °C in air, i.e., 34 °C advancement. Its $T_{d5\%}$ in nitrogen increased even higher to 461 °C from 402 °C, i.e., a 59 °C improvement. The $T_{d5\%}$'s of *m*PEK-*g*-DND samples increased with DND contents. The $T_{d5\%}$'s of *m*PEK-*g*-DND containing 30 wt % of DND were 502 °C in air and 510 °C in nitrogen (Figure 8 and Table 3).

Degree of Polymerization (DP) for the *m*PEK Grafts. On the basis of the experimental results in our model compound study, we have proposed that with an appropriate ether-activated, aromatic carboxylic acid, functionalization of DND via Friedel−Crafts acylation in PPA:P$_2$O$_5$ (w/w 4:1) medium could result in arylcarbonylation of 2.35 carbons in every 100 carbon sites. Furthermore, the arylcarbonylation reaction is most likely to occur at the sp^2 C−H defect sites. On this assumption, we have then determined the upper-limit values for the DP and molecular weight of each VGCNF-bound *m*PEK, ranging from a DP of 5.6 with the corresponding MW of 1099 Da to a DP of 233 and MW of 45 715 Da. Our computation algorithm and results are shown in Table SS-1 (Supporting Information).

Wide-Angle X-ray Diffraction (WAXD). The homopolymer, *m*PEK, is expectedly amorphous as indicated by its featureless WAXD pattern in Figure 9. WAXD scan of the pristine DND reveals diffraction peaks near 44.2° (2θ) as expected for nanocrystalline diamond. This characteristic diamond peak that has appeared at 2.05 Å for all DND-containing samples is attributed to the (111) plane of diamond.[16] As expected, its intensity increases proportionally with the amount of DND present in the samples.

Scanning Electron Microscopy (SEM). SEM images show both pristine and PT-DND could self-organize into clusters or primary aggregates of 20−30 nm size in solid state (Figure 1). Their surfaces are clean and smooth. The surface of 30 wt % *m*PEK-*g*-DND is totally covered with *m*PEK and became rough
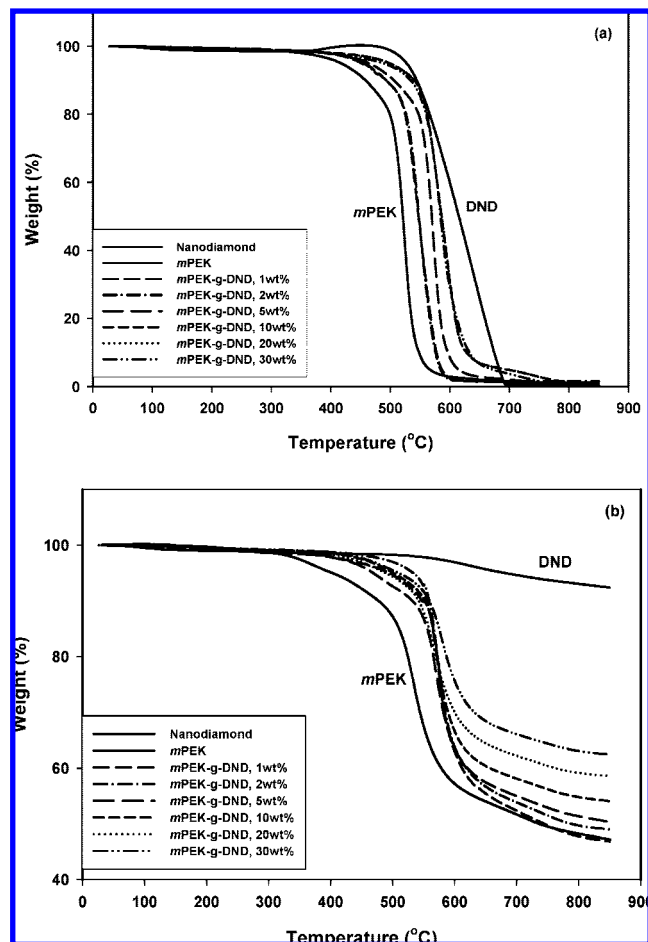
Figure 8. TGA thermograms of *m*PEK-*g*-DND (a) in air and (b) in nitrogen and at a heating rate of 10 °C/min.
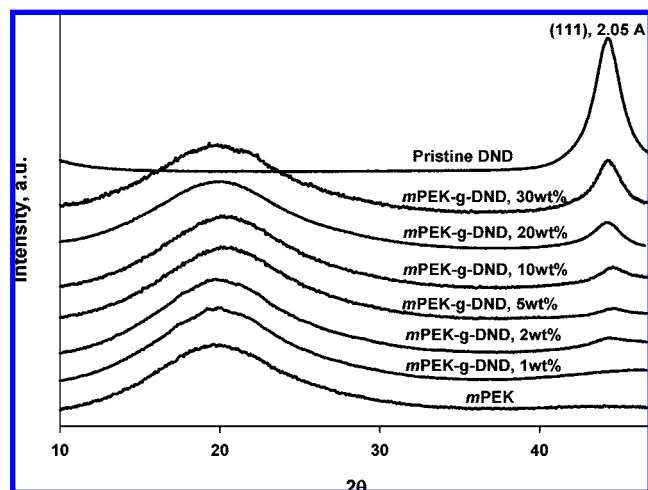

Figure 9. Wide-angle X-ray diffraction patterns of *m*PEK-*g*-DND samples.

and uneven (Figures 10a,b). The cluster sizes are as large as ∼100 nm (Figure 10c). The cluster sizes of 20 wt % *m*PEK-*g*-DND are smaller, ranging from 25 to 50 nm (Figure 10d). These aggregate sizes (25−100 nm) are much larger than both individual nanodiamond (4 nm) particles and their primary aggregates (20−30 nm), providing another piece of evidence that *m*PEK has been grafted onto DND surface.

Transmission Electron Microscope (TEM). The TEM image of pristine DND powder shows that the DND aggregates
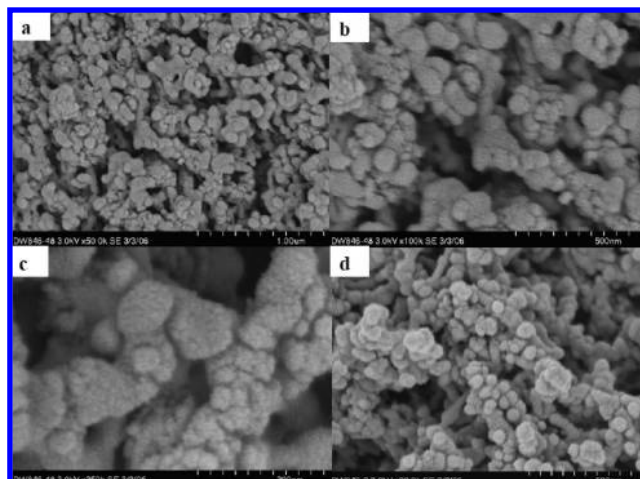

Figure 10. SEM images: (a) *m*PEK-*g*-DND, 30 wt % (×50K); (b) *m*PEK-*g*-DND, 30 wt % (×100K); (c) *m*PEK-*g*-DND, 30 wt % (×250K); (d) *m*PEK-*g*-DND, 20 wt % (×90K). Scale bars are as follows: (a) 1 μm; (b) 500 nm; (c) 200 nm; (d) 500 nm.

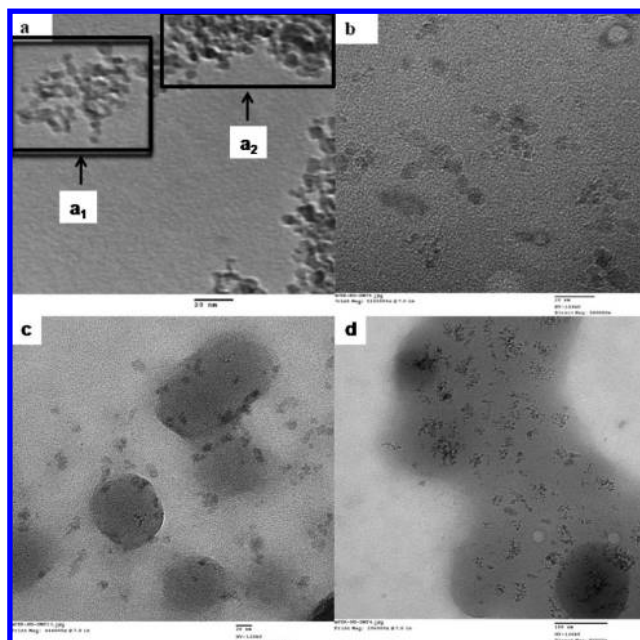**Figure 11.** TEM images obtained for powder samples: (a) pristine DND (×200K), (b) *m*PEK-*g*-DND, 10 wt % (×300K); (c) *m*PEK-*g*-DND, 10 wt % (×120K). The scale bars for images (a), (b), and (c) are 20 nm. Image (d) shows larger area of the same sample of *m*PEK-*g*-DND, 10 wt % (×80K); the scale bar is 100 nm. Note: in (c) and (d), the 100 nm darker spherical spots were formed during the sample drying process. It is possible that *m*PEK-*g*-DND/DMF solution (hydrophilic) might have formed spherical droplets on hydrophobic carbon film. Some smaller droplets (100 nm) might have overlapped forming larger spots.

with average sizes of primary particles around 4 nm in the a₁ region when its concentration is low (Figure 11a). The DND forms much larger aggregates when its concentration is high as shown in the a₂ region of Figure 11a. The TEM images for a 10 wt % *m*PEK-*g*-DND sample (Figures 11b−d) show that DND is quite well dispersed. While some primary DND particles can be observed, most of them are not completely separated, usually a few (3−10) nanoparticles staying together (Figures 11c,d). However, the average sizes of DND are ∼8 nm (Figure 11b), doubling the sizes of pristine DND. This size increase is most probably stemming from the grafting of *m*PEK onto the DND surface.[33] Nevertheless, to our knowledge, these few

individual *m*PEK-grafted nanoparticles are, hitherto, the smallest DND particles observed by TEM in DND-based polymer nanocomposites.

Conclusion

In a number of previous reports, the functionalization chemistry of detonation diamond nanoparticles (in various states of agglomeration) has largely involved the oxygen-containing, surface functional groups such as carboxylic acid and hydroxyl functionalities.[34] Our model reaction indicated that the "aromatic sp^2 C−H"[35] moieties are also present on the primary aggregates and particles. They are accessible for Friedel−Crafts acylation, which is an efficient polymer-forming reaction in PPA/P$_2$O$_5$ medium that both the aromatic sp^2 C−H bonds and CO$_2$H groups can participate in. This is demonstrated by the in-situ polymerization of a suitable AB monomer containing both functionalities in the presence of pristine DND to generate the nanocomposties comprising mainly of (>90 wt %) well-dispersed, polymer-grafted DND, viz. *m*PEK-*g*-DND. While the literature is replete with examples of polymer nanocomposites prepared from the physical blending of as-received DND with various matrix polymers,[36] there are so far only two reported examples of in-situ nanocomposites based on DND, namely the polyaddition of methyl methacrylate via an ATRP process that effectively grafted PMMA from a prefunctionalized DND[15] and grafting an aromatic polyimide from DND via AA + BB type polycondensation process.[16] However, these grafting processes were shown to be only successful on DND agglomerates of larger sizes (20−50 nm). With the caveat that in TEM (Figure 11b−d) images there were tiny aggregates present among the individual polymer-grafted diamond nanoparticles, we believe our work is the first to show the possibility of grafting the DND primary particles (∼4−5 nm) with an aromatic poly(ether−ketone) via an in-situ Friedel−Crafts polycondensation of the corresponding AB monomer. This work reaffirms that polyphosphoric acid with high P$_2$O$_5$ content is indeed quite effective in breaking up the DND agglutinates as well as dispersing and sequestering primary DND particles because of its acidic and viscous character. Together with our previous findings for related VGCNF and MWNT work, this work also reaffirms the prevalence of a common structural feature in these carbon nanomaterials, viz., the "aromatic sp^2 C−H" defect sites[37] that are susceptible to electrophilic reactions such as Friedel−Crafts acylation. On the basis of our experience of working with these carbon nanomaterials, we tentatively conclude that the amount of such defects qualitatively appears to follow the order VGCNF > MWNT > DND. Finally, in a broad sense, this work represents a highly novel example illustrating the coexistence of the hardest and one of the softest matters in a covalently bound system.

Supporting Information Available: (i) Figure SS-1 and Figure SS-1: suspensions of (a) TMPB-*g*-DND and (b) pristine DND in THF after sonication and were allowed to stand at room temperature for a period of 2 weeks; (ii) Figure SS-2: UV−vis absorption spectra of TMPBA, pristine DND, and TMPB-*g*-DND in DMSO; (iii) Figure SS-3: the sample colors of (a) pristine DND, (b) *m*PEK, (c) *m*PEK-*g*-VGCNF, 30 wt %, and (d) *m*PEK-*g*-DND, 30 wt %; (iv) Figure SS-4: molded bar samples of (a) 10 wt % *m*PEK-*g*-DND and (b) 20 wt % *m*PEK-*g*-DND; the dimensions are 2 cm (W) × 6 cm (L) × 0.2 cm (thickness). This material is available free of charge via the Internet at http://pubs.acs.org.

References and Notes

(1) (a) Danilenko, V. V. *Phys. Solid State* **2004**, *46*, 595. (b) Dolmatov, V. Y. *Russ. Chem. Rev.* **2001**, *70*, 607.

(2) Lymkin, A. I.; Petrov, E A.; Ershov, A. P.; Sakovitch, G. V.; Staver, A. M.; Titov, V. M. *Dokl. Akad. Nauk USSR* **1988**, *302*, 611.

(3) Greiner, N. R.; Phillips, D. S.; Johnson, J. D.; Volk, F. *Nature (London)* **1988**, *333*, 440.

(4) Iakoubovskii, K.; Baidakova, M. V.; Wouters, B. H.; Stesmans, A.; Adriaenssens, G. J.; Vul, A. Y.; Grobet, P. J. *Diamond Relat. Mater.* **2000**, *9*, 861, and references therein.

(5) (a) Xu, X.; Yu, Z.; Zhu, Y.; Wang, B. *J. Solid State Chem.* **2005**, *178*, 688. (b) Loktev, V. F.; Makal'skii, V. I.; Stoyanova, I. V.; Kalinkin, A. V.; Likholobov, V. A.; Mit'kin, V. N. *Carbon* **1991**, *29*, 817.

(6) (a) Schrand, A. M.; Dai, L.; Schlager, J. J.; Hussain, S. M.; Ōsawa, E. *Diamond Relat. Mater.* **2007**, *16*, 2118. (b) Schrand, A. M.; Huang, H.; Carlson, C.; Schlager, J. J.; Ōsawa, E.; Hussain, S. M.; Dai, L. *J. Phys. Chem. B* **2007**, *111*, 2. (c) It was also reported that much larger size DND (≥100 nm) had showed low cytotoxicity; see: Yu, S.-J.; Kang, M.-W.; Chang, H.-C.; Chen, K.-M.; Yu, Y.-C. *J. Am. Chem. Soc.* **2005**, *127*, 17604.

(7) (a) Grichko, V. P.; Shenderova, O. A. Nanodiamond: Designing the Bio-Platform In *Ultrananocrystalline Diamond Synthesis, Properties, and Applications*; Shenderova, O. A., Gruen, D. M., Eds.; William Andrew Publishing: Norwich, NY, 2006; pp 529−550. (b) Yeap, W. S.; Tan, Y. Y.; Loh, K. P. *Anal. Chem.* **2008**, *80*, 4659. (c) Fu, C.-C.; Lee, H.-Y.; Chen, K.; Lim, T.-S.; Wu, H.-Y.; Lin, P.-K.; Wei, P.-K.; Tsao, P.-H.; Chang, H.-C.; Fann, W. *Proc. Natl. Acad. Sci. U.S.A.* **2007**, *104*, 727.

(8) (a) Ōsawa, E. *Diamond Relat. Mater.* **2007**, *16*, 2018. (b) *Pure Appl. Chem.* **2008**, 801365.

(9) At the nanoscale level, a recent theoretical study has revealed the importance of electrostatic (Coulombic) interparticle interactions, particularly that between the (111)a and (111)b facets of primary nanodiamonds particles, which are approaching C−C bond energy, in providing the driving force to the self-assembly of nanodiamonds particulates into fibers (1-D) and films (2-D). See: Barnard, A. S. *J. Mater. Chem* **2008**, *18*, 4038.

(10) Huang, H.; Dai, L.; Wang, D. H.; Tan, L.-S.; Osawa, E. *J. Mater. Chem.* **2008**, *18*, 1347.

(11) Krueger, A.; Kataoka, F.; Ozawa, M.; Fujino, T.; Suzuki, Y.; Aleksenskii, A. E.; Vul, A. Y.; Ōsawa, E. *Carbon* **2005**, *43*, 1722.

(12) Liu, Y.; Gu, Z. N.; Margrave, J. L.; Khabashesku, V. N. *Chem. Mater.* **2004**, *16*, 3924.

(13) (a) Liu, Y.; Khabashesku, V. N.; Halas, N. J. *J. Am. Chem. Soc.* **2005**, *127*, 3712.

(14) Mochalin, V. N.; Osswald, S.; Portet, C.; Yushin, G.; Hobson, C.; Havel, M.; Gogotsi, Y. *Mater. Res. Soc. Symp. Proc.* **2008**, 1039 (Diamond Electronics−Fundamentals to Applications II), Paper #: 1039-P11-03.

(15) (a) Krueger, A.; Stegk, J.; Liang, Y.; Lu, L.; Jarre, G. *Langmuir* **2008**, *24*, 4200. (b) Krueger, A. *Chem.−Eur. J.* **2008**, *14*, 1382.

(16) Li, L.; Davidson, J. L.; Lukehart, C. M. *Carbon* **2006**, *44*, 2308.

(17) Zhang, Q.; Natio, K.; Tanaka, Y.; Kagawa, Y. *Macromolecules* **2008**, *41*, 536.

(18) Initial results were described in: Wang, D. H.; Tan, L.-S.; Huang, H.; Dai, L.; Ōsawa, E. *Polym. Prepr.* **2007**, *48* (1), 410.

(19) (a) Ōzawa, M.; Inakuma, M.; Takahashi, M.; Kataoka, F.; Krüger, A.; Ōsawa, E. *Adv. Mater.* **2007**, *19*, 1201. (b) Kavan, L.; Zukalova, M.; Kalbac, M.; Ōsawa, E.; Dunsch, L. *Carbon* **2006**, *44*, 3113. (c) Panich, A. M.; Shames, A. I.; Vieth, H.-M.; Takahashi, M.; Ōsawa, E.; Vul', A. Ya. *Eur. J. Phys. B* **2006**, *52*, 397. (d) Krüger, A.; Kataoka, F.; Ozawa, M.; Fujino, T.; Suzuki, Y.; Aleksenskii, A. E.; Vul', A. Y.; Ōsawa, E. *Carbon* **2005**, *43*, 1722.

(20) (a) Baek, J.-B.; Lyons, C. B.; Tan, L.-S. *J. Mater. Chem.* **2004**, *14*, 2052. (b) Baek, J.-B.; Lyons, C. B.; Tan, L.-S. *Macromolecules* **2004**, *37*, 8278. (c) Baek, J.-B.; Park, S. Y.; Price, G. E.; Lyons, C. B.; Tan, L. S. *Polymer* **2004**, *46*, 1543. (d) Lee, H.-J.; Oh, S.-J.; Choi, J.-Y.; Kim, J. W.; Han, J.; Tan, L.-S.; Baek, J.-B. *Chem. Mater.* **2005**, *17*, 5057. (e) Oh, S.-J.; Lee, H.-J.; Keum, D.-K.; Lee, S.-W.; Wang, D. H.; Park, S.-Y.; Tan, L.-S.; Baek, J.-B. *Polymer* **2006**, *47*, 1132. (f) Wang, D. H.; Baek, J.-B.; Tan, L.-S. *Mater. Sci. Eng. B* **2006**, *132*, 103. (g) Choi, J.-Y.; Oh, S.-J.; Lee, H.-J.; Wang, D. H.; Tan, L.-S.; Baek, J.-B. *Macromolecules* **2007**, *40*, 4474. (h) Wang, D. H.; Arlen, M. J.; Baek, J.-B.; Vaia, R. A.; Tan, L.-S. *Macromolecules* **2007**, *40*, 6100.

(21) Baek, J.-B.; Tan, L.-S. *Polymer* **2003**, *44*, 4135.

(22) Aleksenskii, A. E.; Baidakova, M. V.; Vul', A. Ya.; Siklitskii, V. I. *Phys. Solid State* **1999**, *41*, 668.

(23) Raty, J. Y.; Galli, G.; Bostedt, C.; van Buuren, T. W.; Terminello, L. J. *Phys. Rev. Lett.* **2003**, *90*, 037401.

(24) Barnard, A. S.; Sternberg, M. *J. Phys. Chem. B* **2005**, *109*, 17107.

(25) In a recent report, the results from large-Q neutron diffraction measurements of DND (5 nm) suggest modification of the core−shell model for raw DND with an interlayer of compressed diamond lattice. See: Palosz, B.; Pantea, C.; Grzanka, E.; Stelmakh, S.; Proffen, T.; Zerda, T. W.; Palosz, W. *Diamond Relat. Mater.* **2006**, *15*, 1813.

(26) Osswald, S.; Yushin, G.; Mochalin, V.; Kucheyev, S. O.; Gogotsi, Y. *J. Am. Chem. Soc.* **2006**, *128*, 11635.

(27) The upper limit for C−H defects is ($1.06/7.52 \times 100\%$ =) 14.1 atom % based on 1.06% of hydrogen in DND with the empirical formula $C_{7.52}H_{1.06}N_{0.15}O_{0.30}$ (Table 1). The lower limit of sp^2 C−H defects is 2.7 atom % (14.1 atom % × 19%), and the upper limit of sp^2 C−H defects is 4.2 atom % (14.1 atom % × 30%). Since these values are calculated based on the assumption that there were no OH and NH_2 moieties present in DND, we expect the experimental value for sp^2 C−H defects to be near the lower limit (2.7 atom %).

(28) (a) Shenderova, O. A.; Zhirnov, V. V.; Brenner, D. W. *Crit. Rev. Solid State Mater. Sci.* **2002**, *27*, 227. (b) Jiang, T.; Xu, K.; Ji, S. *J. Chem. Soc., Faraday Trans.* **1996**, *92*, 3401.

(29) It is interesting to note that Krueger et al. reported that weight gains were observed around 500 °C for both pristine DND and OH-functionalized DND samples that were analyzed by TGA in nitrogen. They suggested the possibility of thermochemical incorporation of nitrogen into DND; see ref 15a. In our samples (from a different source), no weight gain was detected by TGA when they were run under nitrogen atmosphere; see also ref 10.

(30) Huang, L. C. L.; Chang, H. C. *Langmuir* **2004**, *20*, 5879.

(31) (a) Wang, X.; Liu, H.; Jin, Y.; Chen, C. *J. Phys. Chem. B* **2006**, *110*, 10236. (b) Hill, D.; Lin, Y.; Qu, L.; Kitaygorodskiy, A.; Connell, J. W.; Allard, L. F.; Sun, Y.-P. *Macromolecules* **2005**, *38*, 7670. (c) Holzinger, M.; Abraham, J.; Whelan, P.; Graupner, R.; Ley, L.; Hennrich, F.; Kappes, M.; Hirsch, A. *J. Am. Chem. Soc.* **2003**, *125*, 8566. (d) Lin, Y.; Rao, A. M.; Sadanadan, B.; Kenik, E. A.; Sun, Y.-P. *J. Phys. Chem. B* **2002**, *106*, 1294. (e) Holzinger, M.; Vostrowsky, O.; Hirsch, A.; Hennrich, F.; Kappes, M.; Weiss, R.; Jellen, F. *Angew. Chem., Int. Ed.* **2001**, *40*, 4002. (f) Sun, Y.-P.; Huang, W.; Lin, Y.; Fu, K.; Kitaygorodskiy, A.; Riddle, L. A.; Yu, Y. J.; Carroll, D. L. *Chem. Mater.* **2001**, *13*, 2864.

(32) Baek, J.-B.; Park, S.-Y.; Price, G. E.; Lyons, C. B.; Tan, L.-S. *Polymer* **2005**, *46*, 1543.

(33) In our TEM of 10 wt % *m*PEK-*g*-DND (Figure 11b), we observed mostly spheroidal entities with diameter of ca. 8 nm. On the basis of a simple geometry argument, one would expect that the smallest aggregate of primary ND particles (spheroidal; ∼4−5 nm); i.e. an aggregate of two should not be spheroidal (one would expect an oblong shape), and the smallest spheroidal aggregate should have a diameter of ca. (3 × 5 nm =) 15 nm, and with polymer shell of ∼3 nm, one would expect the smallest polymer-grafted aggregate would be [15 nm + 2(3 nm) =] 21 nm, instead of ∼8 nm observed.

(34) For recent summaries of DND functionalization efforts:(a) Krueger, A. *Adv. Mater.* **2008**, *20*, 2445. (b) Krueger, A. *J. Mater. Chem.* **2008**, *18*, 1485. (c) Holt, K. B. *Philos. Trans. R. Soc., A* **2007**, *365*, 2845.

(35) From chemical reactivity point of view, an aromatic sp^2 C−H bond is susceptible to electrophilic *substitution* reactions whereas an olefinic sp^2 C−H bond reacts in an electrophilic *addition* fashion.

(36) (a) Dolmatov, V. Y. *Applications of Detonation Nanodiamond*; Shenderova, O. A., Gruen, D. M., Eds.; *Ultrananocrystalline Diamond*; William Andrew Publishing: Norwich, NY, 2006; pp 477−527. (b) Shenderova, O. A.; Tyler, T.; Cunningham, G.; Ray, M.; Walsh, J.; Casulli, M.; Hens, S.; McGuire, G.; Kuznetsov, V.; Lipa, S. *Diamond Relat. Mater.* **2007**, *16*, 1213.

(37) In addition to sp^3 diamond core, it is generally accepted that there are fullerene-like layers, which cover about 30% of the surface of free DND particle, and the carbon atoms, located at the remaining, uncovered spots of the outer surface, are bound to hydrogen and oxygen atoms, producing a variety of functional hydrocarbon groups that saturate the dangling bonds. These shell layers could be detected by C-13 NMR (see ref 19c) and Raman spectroscopy (see ref 19b) even when these layers were not observed by high-resolution TEM. We believe that the dangling (aromatic) sp^2 C−H bonds are the sites where Friedel−Crafts acylation took place.